

Preparation of the Noncentrosymmetric Ferrimagnetic Phase $\text{La}_{0.9}\text{Ba}_{0.1}\text{Mn}_{0.96}\text{O}_{2.43}$ by Topochemical Reduction

Thomas. G. Parsons[†], Joke Hadermann[§], P. Shiv Halasyamani[‡], Michael A. Hayward^{†*}

[†] Department of Chemistry, University of Oxford, Inorganic Chemistry Laboratory, South Parks Road, Oxford, OX1 3QR, UK.

[§]EMAT, University of Antwerp, Groenenborgerlaan 171, B-2020 Antwerp, Belgium.

[‡] Department of Chemistry, University of Houston, 112 Fleming Building, Houston, Texas 77204-5003, USA.

Abstract

Topochemical reduction of $\text{La}_{0.9}\text{Ba}_{0.1}\text{MnO}_3$ with NaH at 225 °C yields the brownmillerite phase $\text{La}_{0.9}\text{Ba}_{0.1}\text{MnO}_{2.5}$. However, reduction with CaH_2 at 435 °C results in the formation of $\text{La}_{0.9}\text{Ba}_{0.1}\text{Mn}_{0.96}\text{O}_{2.43}$ via the deintercalation of both oxide anions and manganese cations from the parent perovskite phase. Electron and neutron diffraction data reveal $\text{La}_{0.9}\text{Ba}_{0.1}\text{Mn}_{0.96}\text{O}_{2.43}$ adopts a complex noncentrosymmetric structure, described in space group *I*23, confirmed by SHG measurements. Low-temperature neutron diffraction data reveal $\text{La}_{0.9}\text{Ba}_{0.1}\text{Mn}_{0.96}\text{O}_{2.43}$ adopts an ordered magnetic structure in which all the nearest neighbor interactions are antiferromagnetic. However, the presence of ordered manganese cation-vacancies results in a net ferrimagnetic structure with net saturated moment of 0.157(2) μB per manganese center.

Keywords: Topochemical reduction; noncentrosymmetric material; magnetism; transition-metal oxides

Highlights

- Topochemical reduction via deintercalation both anions and cations.
- Noncentrosymmetric crystal structure due to anion and cation vacancy order.
- Ordered cation-vacancies result in net ferrimagnetic behavior.

Introduction

The discovery of new extended solids which exhibit noncentrosymmetric (NCS) crystal structures has been a long-standing goal of many chemists because the lack of inversion symmetry is a prerequisite for a number of useful physical properties including ferroelectricity, piezoelectricity and second-harmonic generation (SHG).¹⁻² However, in general it is observed that symmetric packing schemes are energetically more favorable than NCS analogues so centrosymmetric structures tend to be strongly favored, and as a result the discovery of new NCS materials is challenging.

Topochemical synthesis approaches, which utilize differences in ionic mobilities to prepare metastable materials,³⁻⁵ are an attractive option for the preparation of new NCS materials. This is because topochemical reactions operate under kinetic rather than thermodynamic control and as a result tend to form structures which satisfy local bonding requirements, rather than preparing phases which have the minimum global-energy structure. As a consequence, the formation of the most thermodynamically stable centrosymmetric materials can be avoided and metastable, potentially NCS materials prepared. Examples of this approach can be seen in the topochemical oxidation of the centrosymmetric phase Ba_2YFeO_5 to the NCS phase $\text{Ba}_2\text{YFeO}_{5.5}$,⁶⁻⁷ or the topochemical oxidation of $\text{La}_3\text{Ni}_2\text{O}_7$ to $\text{La}_3\text{Ni}_2\text{O}_{5.5}\text{F}_{3.5}$,⁸ although in this later case the inversion symmetry of the phase is broken locally, but not globally.

Here we report the synthesis of $\text{La}_{0.9}\text{Ba}_{0.1}\text{Mn}_{0.96}\text{O}_{2.43}$ which was prepared via the topochemical reduction of $\text{La}_{0.9}\text{Ba}_{0.1}\text{MnO}_3$ during a study of the reduction chemistry of $\text{La}_x\text{A}_{1-x}\text{MnO}_3$ perovskite phases.⁹ We were initially unable to deduce the structure of this non-centrosymmetric phase, however a recent report of an isostructural phase $\text{Tb}_{0.5}\text{Ca}_{0.5}\text{Mn}_{0.96}\text{O}_{2.37}$ by Zhang *et al.*¹⁰ allowed us to determine the crystal structure of $\text{La}_{0.9}\text{Ba}_{0.1}\text{Mn}_{0.96}\text{O}_{2.43}$ by analogy, and then the low-temperature magnetic structure of the phase.

Experimental Section

Synthesis of $\text{La}_{0.9}\text{Ba}_{0.1}\text{MnO}_3$. Samples of $\text{La}_{0.9}\text{Ba}_{0.1}\text{MnO}_3$ were prepared using a citrate gel method. Appropriate quantities of La_2O_3 (99.999%, dried at 900 °C), BaCO_3 (99.997%), and MnO_2 (99.999%) were dissolved in a 1:1 mixture of concentrated nitric acid and distilled water. Citric acid and ethylene glycol were added, and the solution was heated whilst being stirred. The gels thus formed were allowed to combust in air and the subsequent products were ground into a fine powder, placed in alumina crucibles and heated in air, at a rate of 1 °C min⁻¹ to 900 °C, to remove the organic components from the samples. The resulting powders were ground, pressed into pellets and heated under flowing argon at 1500 °C for 2 periods of 24 h, with intermediate regrinding. The samples were then ground into a fine powder and heated at 400 °C under flowing oxygen. Samples were observed to be phase pure by laboratory X-ray powder diffraction with lattice parameters in good agreement with published values.¹¹

Topochemical reduction of $\text{La}_{0.9}\text{Ba}_{0.1}\text{MnO}_3$. A sample of approximately 5g of $\text{La}_{0.9}\text{Ba}_{0.1}\text{MnO}_3$ was ground together with 2 mole equivalents of NaH (99 %) in an argon filled glovebox. The powdered mixture was then sealed in an evacuated Pyrex ampoule and heated for 2 d periods sequentially at 200 °C, 210 °C, 215 °C and 225 °C. The reaction was deemed complete when its diffraction pattern did not change between heating cycles, at this stage the sample were then washed with 4 x 100 ml of methanol under nitrogen to remove sodium containing by-products (NaOH and NaH) before being dried under vacuum. This will be referred to as reduced sample A. Heating samples of $\text{La}_{0.9}\text{Ba}_{0.1}\text{MnO}_3$ with NaH above 235 °C led to sample decomposition and the formation of La_2O_3 , MnO and other amorphous products.

An additional reduced sample was prepared by mixing approximately 5g of $\text{La}_{0.9}\text{Ba}_{0.1}\text{MnO}_3$ with 1 mole equivalent of CaH_2 (99%) in an argon filled glovebox. The powder mixture was placed in a ‘venting’ apparatus to mitigate the release of H_2 gas, described previously,¹² and then heated at 350 °C for 24 h and then 400 °C for 2 periods of 24 h. At this stage an additional 0.5 mole equivalents of CaH_2 was added to the reaction mixture and it was heated for 24 h at 425 °C and then 435 °C, with grinding between heating periods. The reaction mixture was then washed under nitrogen with 4 x 100 ml of a 0.1 M NH_4Cl solution in methanol to remove calcium containing by-products (CaO and CaH_2) and then 3 x 100 ml of methanol to remove the NH_4Cl residues, before being dried under vacuum. This will be referred to as reduced sample B. Heating samples of $\text{La}_{0.9}\text{Ba}_{0.1}\text{MnO}_3$ with CaH_2 below 300 °C led to no observable reaction.

Characterization. X-ray powder diffraction data were collected using a PANalytical X'Pert diffractometer incorporating an X'celerator position sensitive detector (monochromatic Cu K $_{\alpha 1}$ radiation). Data were collected from air sensitive samples under an inert atmosphere using a homemade gas-tight sample holder. Neutron powder diffraction data were collected using the D2b diffractometer ($\lambda = 1.59 \text{ \AA}$) at the ILL neutron source, Grenoble from samples sealed under argon in vanadium cans. Rietveld profile refinement was performed using the GSAS suite of programs.¹³ Samples for electron microscopy investigation were prepared by crushing the powder sample in ethanol and depositing it on a holey carbon grid. Electron diffraction (ED) studies were performed using a Philips CM20 microscope. Thermogravimetric reoxidation measurements were performed by heating powdered samples under flowing oxygen using a Netzsch STA 409PC balance. Average manganese oxidation states were determined by iodometric titration. Samples were dissolved in HCl containing an excess of KI and the liberated I $_2$ was titrated with Na $_2$ S $_2$ O $_3$. The powder SHG response of samples was recorded and compared to a standard sample of α -SiO $_2$. No index matching fluid was used in any of the experiments. A detailed description of the experimental setup and process has been reported previously.¹⁴

Results

Structural and compositional characterization of La $_{0.9}$ Ba $_{0.1}$ MnO $_{2.5}$. X-ray powder diffraction data collected from reduced sample A can be indexed using a body-centered orthorhombic unit cell ($a = 5.63 \text{ \AA}$, $b = 16.23 \text{ \AA}$, $c = 5.61 \text{ \AA}$) consistent with the formation of an anion-vacancy ordered brownmillerite phase. Thermogravimetric data collected during the reoxidation of sample A back to La $_{0.9}$ Ba $_{0.1}$ MnO $_3$ (confirmed by X-ray powder diffraction) indicated a composition of La $_{0.9}$ Ba $_{0.1}$ MnO $_{2.51(2)}$, as shown in Figure S1, again consistent with a brownmillerite phase. Sample A will henceforth be referred to as La $_{0.9}$ Ba $_{0.1}$ MnO $_{2.5}$.

Neutron powder diffraction data could also be indexed using the cell obtained from the X-ray diffraction data, so three brownmillerite structural models in space groups $I2mb$, $Imma$ and $Pnma$, utilized previously to describe manganese based brownmillerite phases,⁹ were refined against the neutron powder diffraction data. Inspection of the fits to the data revealed a series of diffraction peaks which could be attributed to a small quantity (~ 5 weight %) of unreduced La $_{0.9}$ Ba $_{0.1}$ MnO $_3$, so this was added to the models as a second phase. The model described in space group $Imma$ gave the best numerical and visual fit to the data (See Table S1 in the Supporting Information). Full details of the refined model are given in Table 1, with selected bond lengths in Table S2 and a plot of the observed and calculated data in shown in Figure 1.

Magnetic characterization of La $_{0.9}$ Ba $_{0.1}$ MnO $_{2.5}$. Zero-field cooled (ZFC) and field cooled (FC) magnetization data collected from La $_{0.9}$ Ba $_{0.1}$ MnO $_{2.5}$ in an applied field of 100 Oe (Figure 2) can be fitted by the Curie-Weiss law in the temperature range $210 < T/K < 300$ to yield values of $C = 3.81(2) \text{ cm}^3 \text{ K mol}^{-1}$ and $\theta = -162.5(9) \text{ K}$. The observed value of the Curie constant is approximately what would be expected for the combination of $S = 5/2 \text{ Mn}^{2+}$ and $S = 2 \text{ Mn}^{2+}$ given by the La $_{0.9}$ Ba $_{0.1}$ MnO $_{2.5}$ chemical formula ($C_{\text{expected}} = 4.23 \text{ cm}^3 \text{ K mol}^{-1}$). Below $T \sim 175 \text{ K}$ the ZFC and FC data diverge, with the ZFC data exhibiting a local maximum at $T \sim 15 \text{ K}$.

Neutron powder diffraction data collected from La $_{0.9}$ Ba $_{0.1}$ MnO $_{2.5}$ show additional diffraction features compared to the analogous data collected at 300 K. These additional features can be indexed using the orthorhombic unit cell of the unreduced La $_{0.9}$ Ba $_{0.1}$ MnO $_3$ starting material, and the intensities of these reflections can be fitted using a G-type antiferromagnetic model, with an ordered moment of $4.2(3) \mu_B$ per manganese. As a result, we can conclude that there is no indication of long-range magnetic order in the majority La $_{0.9}$ Ba $_{0.1}$ MnO $_{2.5}$ phase. Plots of the observed and calculated data are shown in Figure S2 in the Supporting Information, along with a complete description of the refined magnetic model in Table S3.

Structural and compositional characterization of La $_{0.9}$ Ba $_{0.1}$ Mn $_{0.96}$ O $_{2.43}$. X-ray and neutron powder diffraction data collected from reduced sample B can be indexed using a body-centered cubic unit cell ($a = 15.985 \text{ \AA}$). Thermogravimetric data collected during the reoxidation of sample B back to La $_{0.9}$ Ba $_{0.1}$ MnO $_3$ (confirmed by X-ray powder diffraction) indicated a composition of La $_{0.9}$ Ba $_{0.1}$ MnO $_{2.41(2)}$, as shown in Figure S4. To confirm this low oxygen content, iodometric titrations were performed on reduced sample B, which indicated a composition of La $_{0.9}$ Ba $_{0.1}$ MnO $_{2.43(3)}$, confirming the thermogravimetric data.

To gain more crystallographic information on ‘La_{0.9}Ba_{0.1}MnO_{2.41}’, electron diffraction data were collected, and as shown in Figure 3a the diffraction patterns confirm the cubic, body-centered unit cell determined from the X-ray and neutron diffraction data. Close examination of these data revealed that the only extinction conditions which could be extracted are $h + k + l = 2n$, giving the extinction symbol $I_{- - -}$, consistent with 6 space groups ($I23$ (#197), $I2_13$ (#199), $Im\bar{3}$ (#204), $I432$ (#211), $\bar{I}43m$ (#217) and $Im\bar{3}m$ (#229)).

To narrow this list down, precession electron diffraction (PED) patterns were collected to further probe the symmetry of the unit cell. As shown in Figure 3b, the PED data reveal the absence of a mirror plane perpendicular to $\langle 110 \rangle$ in diffraction patterns from $\langle uuv \rangle$ zone axes. This indicates the Laue class is $m\bar{3}$ not $m\bar{3}m$, reducing the list of possible space groups to $I23$ (#197), $I2_13$ (#199) and $Im\bar{3}$ (#204). A series of structural models were constructed based on a $4 \times 4 \times 4$ geometric expansion of the simple perovskite unit cell with ordered anion vacancies. However, none of the models fitted the X-ray or neutron diffraction data well. As a result we were unable to determine the structure of ‘La_{0.9}Ba_{0.1}MnO_{2.41}’ until recently when Zhang *et al.* reported the structure of Tb_{0.5}Ca_{0.5}Mn_{0.96}O_{2.37},¹⁰ a phase prepared by the topochemical reduction of Tb_{0.5}Ca_{0.5}Mn_{0.96}O₃ and observed to adopt a structure described in space group $I23$ with a lattice parameter of $a = 15.27$ Å. The similarity between the features of Tb_{0.5}Ca_{0.5}Mn_{0.96}O_{2.37} and ‘La_{0.9}Ba_{0.1}MnO_{2.41}’ encouraged us to construct a model based on the reported structure of Tb_{0.5}Ca_{0.5}Mn_{0.96}O_{2.37}, but with a La/Ba solid solution on the A-cation site, and refine this model simultaneously against X-ray and neutron powder diffraction data collected from ‘La_{0.9}Ba_{0.1}MnO_{2.41}’. All atomic positional and displacement parameters were allowed to refine freely, and the model refined smoothly to give a good fit to the diffraction data indicating that La_{0.9}Ba_{0.1}MnO_{2.41} is isostructural with Tb_{0.5}Ca_{0.5}Mn_{0.96}O_{2.37}. A complete description of the refined model is given in Table 2, with selected bond lengths in Table S4 and a plot of the observed and calculated data shown in Figure 4. In common with the Tb/Ca phase, the unit cell contents of the refined structure of ‘La_{0.9}Ba_{0.1}MnO_{2.41}’ is (La_{0.9}Ba_{0.1})₆₄Mn₆₂O₁₅₆, giving a ‘perovskite’ composition of La_{0.9}Ba_{0.1}Mn_{0.96}O_{2.43}. Sample B will henceforth be referred to as La_{0.9}Ba_{0.1}Mn_{0.96}O_{2.43}. A representation of the refined structure of La_{0.9}Ba_{0.1}Mn_{0.96}O_{2.43} is shown in Figure 5a. Powder SHG measurements indicate that La_{0.9}Ba_{0.1}Mn_{0.96}O_{2.43} has an SHG response which is approximately half that of α -SiO₂, consistent with the refined NCS structure. It should be noted that the sample is slightly absorbing at the wavelength used for the SHG measurements, so this value may underestimate the SHG activity of the phase.

Magnetic characterization of La_{0.9}Ba_{0.1}Mn_{0.96}O_{2.43}. Magnetization data collected from La_{0.9}Ba_{0.1}Mn_{0.96}O_{2.43} as a function of temperature (Figure 6) can be fit by the Curie-Weiss law in the temperature range $200 < T/K < 300$ to yield values of $C = 4.65(3) \text{ cm}^3 \text{ K mol}^{-1}$ and $\theta = -391(4) \text{ K}$. The observed value of the Curie constant is a little larger than the expected value based on a mixture of Mn²⁺ and Mn³⁺ defined by the chemical composition ($C_{\text{calc}} = 4.32 \text{ cm}^3 \text{ K mol}^{-1}$). On cooling below 200 K the ZFC and FC data diverge weakly and show anomalies at 165 K and 125 K, most clearly seen in the inset to Figure 6. We are not able to say very much about the nature of these anomalies, but we note that MnO and La_{0.9}Ba_{0.1}MnO_{2.5} (likely impurity phases) exhibit magnetic ordering events at $T_N \sim 120 \text{ K}$ ¹⁵ and 170 K (Figure 2) respectively, so it is likely these magnetic features are due to very small quantities of impurity phases which are not observable by diffraction. Magnetization data collected at 5 K as a function of applied field (Figure 6) suggest ferromagnetic or ferrimagnetic behavior. Linear fits to the high field data ($H > 2T$) yield a saturated moment of $0.157(2) \mu\text{B}$ per manganese.

Neutron powder diffraction data collected from La_{0.9}Ba_{0.1}Mn_{0.96}O_{2.43} at 5K (Figure 7) exhibit additional features compared to the analogous data collected at room temperature (Figure 4), indicative of magnetic order. These additional diffraction peaks can be indexed using the crystallographic unit cell, with intensities best accounted for by the modified G-type antiferromagnetic model shown in Figure 5d, with an ordered moment of $4.34(2) \mu\text{B}$ per manganese center. During the refinement of the magnetic structure the magnitude of the ordered moments was constrained to be the same for all the manganese centers, despite there being 5 crystallographically distinct sets of manganese cations (Mn(1)-(5)), because any attempt to lift this constraint led to refinement instability. Full details of the refined magnetic structure of La_{0.9}Ba_{0.1}Mn_{0.96}O_{2.43} are given in the supporting information.

The magnetic structure shown in Figure 5d reveals that if a G-type antiferromagnetic arrangement, in which all the nearest-neighbor interactions are antiferromagnetic, is applied to the unit cell of La_{0.9}Ba_{0.1}Mn_{0.96}O_{2.43}, the ‘missing’ manganese cations at the origin and body-center of the cell lead to a mismatch in the number of ‘up’

and ‘down’ ordered spins. As a result, $\text{La}_{0.9}\text{Ba}_{0.1}\text{Mn}_{0.96}\text{O}_{2.43}$ can be considered to have a ferrimagnetic structure with a net ordered moment of $2 \times 4.34 = 8.68 \mu\text{B}$ per unit cell or $0.14 \mu\text{B}$ per manganese center, in good agreement with the high-field saturated moment of $0.157(2) \mu\text{B}$ per manganese obtained from the magnetization data.

Discussion

Reaction between $\text{La}_{0.9}\text{Ba}_{0.1}\text{MnO}_3$ and NaH at temperatures up to 225°C results in the topochemical deintercalation of oxide ions from the perovskite framework and the formation of the brownmillerite phase $\text{La}_{0.9}\text{Ba}_{0.1}\text{MnO}_{2.5}$. There are a number of variants of the brownmillerite structure which differ in their arrangement of the distorted chains of MnO_4 tetrahedra within the 3D framework.⁹ The particular brownmillerite structural variant adopted by a phase can be rationalized on the basis of the magnitude of the twisting distortion to the chains of tetrahedra, and the size of the separation between the layers of tetrahedra. As reported previously both the degree of chain distortion (parameterized as $180^\circ - \text{O}(3)-\text{O}(3)-\text{O}(3)$) and the interlayer separation (parameterized as half the b lattice parameter) decline with decreasing x in the $\text{La}_{1-x}\text{A}_x\text{MnO}_{2.5}$ ($\text{A} = \text{Ba}, \text{Sr}, \text{Ca}$) series of brownmillerite phases.⁹ The values of the interlayer separation and the degree of chain distortion observed for $\text{La}_{0.9}\text{Ba}_{0.1}\text{MnO}_{2.5}$ are consistent with the trends in these values observed for other $\text{La}_x\text{Ba}_{1-x}\text{MnO}_{2.5}$ phases ($0.167 < x < 0.3$).⁹ Furthermore the decrease observed in both parameters is also consistent with the change from the *I2mb* variant at $x = 0.167$ to the *Imma* variant for the $x = 0.1$ phase reported here.

The lack of long-range magnetic order in $\text{La}_{0.9}\text{Ba}_{0.1}\text{MnO}_{2.5}$, as indicated by the lack of magnetic Bragg scattering in low-temperature neutron diffraction data, can be attributed to the mixed-valent $\text{Mn}^{2+/3+}$ oxidation state of the phase. As noted in other topochemically reduced manganese perovskite oxides, there is a strong preference for locating Mn^{3+} centers in octahedral rather than tetrahedral coordination sites.¹⁶⁻¹⁷ This means that the octahedrally coordinated manganese cations in $\text{La}_{0.9}\text{Ba}_{0.1}\text{MnO}_{2.5}$ have a 4:1 $\text{Mn}^{2+}:\text{Mn}^{3+}$ ratio. Furthermore, the axial elongation of the $\text{Mn}(1)\text{O}_6$ octahedra mean that the empty $\text{dx}^2\text{-y}^2$ orbitals of the Mn^{3+} centers will lie in the ac -plane of $\text{La}_{0.9}\text{Ba}_{0.1}\text{MnO}_{2.5}$ and as a result the in-plane $\text{Mn}^{3+}-\text{O}-\text{Mn}^{2+}$ super-exchange couplings will be ferromagnetic, while the corresponding $\text{Mn}^{2+}-\text{O}-\text{Mn}^{2+}$ and $\text{Mn}^{3+}-\text{O}-\text{Mn}^{3+}$ couplings will be antiferromagnetic, as will the inter-layer super-exchange couplings between $\text{Mn}(1)\text{O}_6$ and $\text{Mn}(2)\text{O}_4$ units. This combination of conflicting ferromagnetic and antiferromagnetic couplings may be expected to lead to a spin-glass state. However, magnetization-field isotherms collected from $\text{La}_{0.9}\text{Ba}_{0.1}\text{MnO}_{2.5}$ after field cooling are symmetric about the origin (Figure S3), contradicting this possibility. Therefore, we conclude that while the conflicting magnetic couplings in $\text{La}_{0.9}\text{Ba}_{0.1}\text{MnO}_{2.5}$ do not lead to spin-glass behavior, they do limit the length scale of any magnetically ordered state to dimensions which are too small to yield magnetic Bragg scattering.

Reaction between $\text{La}_{0.9}\text{Ba}_{0.1}\text{MnO}_3$ and CaH_2 at 435°C results in the topochemical extraction of both oxide anions and manganese cations, to form a non-centrosymmetric phase with composition $\text{La}_{0.9}\text{Ba}_{0.1}\text{Mn}_{0.96}\text{O}_{2.43}$. The structure of $\text{La}_{0.9}\text{Ba}_{0.1}\text{Mn}_{0.96}\text{O}_{2.43}$ is complex. From the perspective of the La/Ba and Mn cations, it can be considered as a $4 \times 4 \times 4$ expansion of the aristotype perovskite unit cell from which manganese cations have been removed from the origin and cell-center to give a $(\text{La}_{0.9}\text{Ba}_{0.1})_{64}\text{Mn}_{62}$ cation composition. The anion framework has also undergone significant rearrangement so that the MnO_x polyhedra are connected by a combination of edge and corner sharing, compared to the all corner-shared network of MnO_6 octahedra in the parent perovskite phase.

One way to consider the structure of $\text{La}_{0.9}\text{Ba}_{0.1}\text{Mn}_{0.96}\text{O}_{2.43}$ is to observe that each ‘vacant’ manganese cation site sites at the center of a cube of 8 $\text{Mn}(5)\text{O}_6$ octahedra, as shown in Figure 8a. The edges of each Mn-vacancy-centered cube are made from $\text{Mn}(1)\text{O}_5$ units which link with the $\text{Mn}(5)\text{O}_6$ octahedra through shared oxide ions, and each face of the Mn-vacancy-centered cube is completed by a $\text{Mn}(3)\text{O}_4$ unit which is apex-linked to the $\text{Mn}(1)\text{O}_5$ units, as shown in Figure 8b. The body-centered array of Mn vacancies leads to an apex-linked array of the Mn-vacancy-centered cubes as shown in Figure 8c and schematically in Figure 8d. The structure is completed by bands of apex- and edge-linked $\text{Mn}(2)\text{O}_6$ octahedra and $\text{Mn}(4)\text{O}_5$ units which reside in the spaces between the Mn-vacancy-centered cubes as shown in Figure 8e, resulting in a complex network of linked Mn-centered coordination polyhedra.

The conversion of $\text{La}_{0.9}\text{Ba}_{0.1}\text{MnO}_3$ to $\text{La}_{0.9}\text{Ba}_{0.1}\text{Mn}_{0.96}\text{O}_{2.43}$ lifts the inversion symmetry of the framework, with the reduced phase described in space group $I23$ (#197). The symmetry breaking on reduction can be attributed to

a combination of the anion vacancy ordering and the tilting distortions of the resulting MnO_x polyhedra as described previously for $\text{Tb}_{0.5}\text{Ca}_{0.5}\text{Mn}_{0.96}\text{O}_{2.37}$.¹⁰

While $\text{Tb}_{0.5}\text{Ca}_{0.5}\text{Mn}_{0.96}\text{O}_{2.37}$ and $\text{La}_{0.9}\text{Ba}_{0.1}\text{Mn}_{0.96}\text{O}_{2.43}$ are isostructural, they exhibit strikingly different chemical stability. Zhang *et al.* report that $\text{Tb}_{0.5}\text{Ca}_{0.5}\text{Mn}_{0.96}\text{O}_{2.37}$ can only be prepared by reacting $\text{Tb}_{0.5}\text{Ca}_{0.5}\text{Mn}_{0.96}\text{O}_3$ with NaH at 210 °C for 14 days, and that raising the temperature to 230 °C leads to decomposition of the phase.¹⁰ In contrast reaction of $\text{La}_{0.9}\text{Ba}_{0.1}\text{MnO}_3$ with NaH at 210 °C yields a brownmillerite phase, with $\text{La}_{0.9}\text{Ba}_{0.1}\text{Mn}_{0.96}\text{O}_{2.43}$ only observed after reaction with CaH_2 at 435 °C. This lower reactivity and apparently greater thermal stability can be attributed to a combination of two factors. Firstly, the A-site cations in the (La/Ba) MnO_x system are much larger than those in the (Tb/Ca) MnO_x system and as a result the Mn–O framework in the later system will be under more strain and be more distorted, potentially destabilizing the reduced phase. Secondly, the average manganese oxidation state is lower in $\text{La}_{0.9}\text{Ba}_{0.1}\text{Mn}_{0.96}\text{O}_{2.43}$ ($\text{Mn}^{+2.04}$) compared to $\text{Tb}_{0.5}\text{Ca}_{0.5}\text{Mn}_{0.96}\text{O}_{2.37}$ ($\text{Mn}^{+2.33}$) and as a consequence further reduction of $\text{La}_{0.9}\text{Ba}_{0.1}\text{Mn}_{0.96}\text{O}_{2.43}$ is potentially suppressed leading to greater thermal stability.

Conclusion.

The topochemical reduction of $\text{La}_{0.9}\text{Ba}_{0.1}\text{MnO}_3$ yields $\text{La}_{0.9}\text{Ba}_{0.1}\text{Mn}_{0.96}\text{O}_{2.43}$ via the deintercalation of both oxide anions and manganese cations. The ordering of the cation and anion vacancies in combination with tilting distortions of the MnO_x coordination polyhedra breaks the inversion symmetry of the perovskite lattice, demonstrated by the observation of SHG activity. The presence of ordered manganese cation-vacancies changes what would be a simple G-type antiferromagnetic structure into a ferrimagnetic arrangement, further illustrating the influence the ordered cation and anion vacancies have on the physical properties of the phase.

Acknowledgments.

We thank the EPSRC for funding this work and E. Suard for assisting with the collection of the neutron powder diffraction data. PSH thanks the Welch Foundation (Grant E-1457) for support.

Supplementary Information.

Thermogravimetric reoxidation data from $\text{La}_{0.9}\text{Ba}_{0.1}\text{MnO}_{2.5}$ and $\text{La}_{0.9}\text{Ba}_{0.1}\text{Mn}_{0.96}\text{O}_{2.43}$; selected bond lengths from the refined structures of $\text{La}_{0.9}\text{Ba}_{0.1}\text{MnO}_{2.5}$ and $\text{La}_{0.9}\text{Ba}_{0.1}\text{Mn}_{0.96}\text{O}_{2.43}$; Fitting statistics from the structural refinement of $\text{La}_{0.9}\text{Ba}_{0.1}\text{MnO}_{2.50}$; Observed, calculated and difference plots and refined parameters from the structural refinement of $\text{La}_{0.9}\text{Ba}_{0.1}\text{MnO}_{2.5}$ against neutron powder diffraction data collected at 5K; Magnetisation-field isotherms collected from $\text{La}_{0.9}\text{Ba}_{0.1}\text{MnO}_{2.5}$ at 300 K and 5 K after field-cooling in 50,000 Oe.

References

1. Lines, M. E.; Glass, A. M., *Principles and Applications of Ferroelectrics and Related Materials*. Oxford University Press: Oxford, 1991.
2. Nye, F. J., *Physical Properties of Crystals*. Oxford University Press: Oxford, UK, 1957.
3. Hayward, M. A., Soft chemistry synthesis of oxides. In *Comprehensive Inorganic Chemistry II*, Reedijk, J.; Poeppelmeier, K. R., Eds. Elsevier: Oxford, 2013; Vol. 2, pp 417-453.
4. Schaak, R. E.; Mallouk, T. E., Perovskites by design: A toolbox of solid-state reactions. *Chem. Mater.* **2002**, *14* (4), 1455-1471.
5. Ranmohotti, K. G. S.; Josepha, E.; Choi, J.; Zhang, J. X.; Wiley, J. B., Topochemical Manipulation of Perovskites: Low-Temperature Reaction Strategies for Directing Structure and Properties. *Adv. Mater.* **2011**, *23* (4), 442-460.
6. Luo, K.; Hayward, M. A., Complex cation order in anion-deficient $\text{Ba}_n\text{YFe}_{n-1}\text{O}_{2.5n}$ perovskite phases. *Inorg. Chem.* **2012**, *51*, 12281-12287.
7. Luo, K.; Johnson, R. D.; Tran, T. T.; Halasyamani, P. S.; Radaelli, P. G.; Hayward, M. A., $\text{Ba}_2\text{YFeO}_{5.5}$: A Ferromagnetic Pyroelectric Phase Prepared by Topochemical Oxidation. *Chem. Mater.* **2013**, *25* (9), 1800-1808.
8. Zhang, R.; Senn, M. S.; Hayward, M. A., Directed Lifting of Inversion Symmetry in Ruddlesden-Popper Oxide-Fluorides: Toward Ferroelectric and Multiferroic Behavior. *Chem. Mater.* **2016**, *28* (22), 8399-8406.
9. Parsons, T. G.; D'Hondt, H.; Hadermann, J.; Hayward, M. A., The synthesis and structural characterisation of $\text{La}_{1-x}\text{A}_x\text{MnO}_{2.5}$ (A = Ba, Sr, Ca) phases – mapping the variants of the brownmillerite structure. *Chem. Mater.* **2009**, *21*, 5527-5538.
10. Zhang, H.; Gao, S.; Zhang, Q. H.; Wu, J. E.; Liang, J.; Dong, C.; Gu, L.; Dong, S. X.; Sun, J. L.; Liao, F. H.; Lin, J. H.; Zou, R. Q.; Li, G. B., Topotactic Reduction toward a Noncentrosymmetric Deficient Perovskite $\text{Tb}_{0.50}\text{Ca}_{0.50}\text{Mn}_{0.96}\text{O}_{2.37}$ with Ordered Mn Vacancies and Piezoelectric Behavior. *Chem. Mater.* **2017**, *29* (22), 9840-9850.
11. Dabrowski, B.; Rogacki, K.; Xiong, X.; Klamut, P. W.; Dybziński, R.; Shaffer, J., synthesis and properties of vacancy free $\text{La}_{1-x}\text{Ba}_x\text{MnO}_3$. *Phys. Rev. B* **1998**, *58*, 2716-2723.
12. O'Malley, M.; Lockett, M. A.; Hayward, M. A., Anion vacancy ordering in $\text{Sr}_7\text{Mn}_4\text{O}_{15-x}$ phases. *J. Solid State Chem.* **2007**, *180*, 2851-2858.
13. Larson, A. C.; Von Dreele, R. B. *General Structure Analysis System*, Los Alamos National Laboratory Report LAUR 86-748: 2000.
14. Ok, K. M.; Chi, E. O.; Halasyamani, P. S., Bulk characterization methods for non-centrosymmetric materials: second-harmonic generation, piezoelectricity, pyroelectricity, and ferroelectricity. *Chem. Soc. Rev.* **2006**, *35*, 710-717.
15. Goodenough, J. B.; Longo, J. M., *Landolt-Börnstein Tabellen*. Springer: Berlin, Heidelberg, New York, 1970; p 228.
16. Dixon, E.; Hadermann, J.; Hayward, M. A., The synthesis and complex anion-vacancy ordered structure of $\text{La}_{0.33}\text{Sr}_{0.67}\text{MnO}_{2.42}$. *J. Solid State Chem.* **2011**, *184*, 1791-1799.
17. Dixon, E.; Hadermann, J.; Hayward, M. A., Structures and magnetism of $\text{La}_{1-x}\text{Sr}_x\text{MnO}_{3-(0.5+x)/2}$ ($0.67 \leq x \leq 1$) Phases. *Chem. Mater.* **2012**, *24* (8), 1486-1495.

TABLES

Atom	symmetry	x	y	z	Fraction	U _{iso} (Å ²)
La/Ba	8h	0	0.1144(2)	0.485(1)	0.9/0.1	0.015(1)
Mn(1)	4a	0	0	0	1	0.004(1)
Mn(2)	8i	0.054(2)	¼	0.975(2)	½	0.005(1)
O(1)	8g	¼	0.9881(4)	¼	1	0.021(1)
O(2)	16j	0.038(2)	0.1371(4)	0.072(1)	½	0.021(1)
O(3)	8i	0.874(3)	¼	0.609(3)	½	0.021(1)
La _{0.9} Ba _{0.1} MnO _{2.5} - Space Group: <i>Imma</i> (#74) Formula weight = 233.69 g mol ⁻¹ $a = 5.6320(9)$ Å, $b = 16.2344(15)$ Å, $c = 5.6188(9)$ Å, volume = 513.7(1) Å ³ 94.3(5) weight %						
La _{0.9} Ba _{0.1} MnO ₃ - Space Group: <i>Pnma</i> (#62) Formula weight = 241.69 g mol ⁻¹ $a = 5.578(5)$ Å, $b = 7.796(9)$ Å, $c = 5.544(5)$ Å, volume = 241.1(2) Å ³ 5.7(5) weight %						
Radiation source: Neutron, $\lambda = 1.594$ Å Temperature: Room temperature $\chi^2 = 1.271$; $wRp = 6.26$ %; $Rp = 4.88$ %.						

Table 1. Structural parameters from the refinement of La_{0.9}Ba_{0.1}MnO_{2.5} against neutron powder diffraction data collected at room temperature.

Atom	symmetry	x	y	z	Fraction	U _{iso} (Å ²)
La/Ba (1)	8c	0.1340(8)	0.1340(8)	0.1340(8)	0.9/0.1	0.033(5)
La/Ba (2)	24f	0.3782(8)	0.1505(5)	0.1126(7)	0.9/0.1	0.019(2)
La/Ba (3)	24f	0.6204(6)	0.1488(5)	0.1147(6)	0.9/0.1	0.008(1)
La/Ba (4)	8c	0.8646(6)	0.1353(6)	0.1353(6)	0.9/0.1	0.012(3)
Mn (1)	24f	0.0004(25)	0.2301(5)	0.7520(5)	1	0.014(2)
Mn (2)	6b	½	0	0	1	0.036(5)
Mn (3)	12d	0	0	0.2523(8)	1	0.015(2)
Mn (4)	12e	0.1999(6)	½	0	1	0.009(2)
Mn (5)	8c	0.2494(27)	0.2494(27)	0.2494(27)	1	0.011(2)
O (1)	24f	0.5001(25)	0.3944(5)	0.0920(4)	1	0.046(2)
O (2)	24f	0.3773(6)	0.7217(5)	0.7818(6)	1	0.004(1)
O (3)	12e	½	0.1459(5)	0	1	0.022(2)
O (4)	24f	0.1203(8)	0.2232(7)	0.2690(7)	1	0.025(2)
O (5)	24f	0.0037(12)	0.7185(4)	0.1249(3)	1	0.018(1)
O (6)	24f	0.6283(3)	0.2851(3)	0.0014(12)	1	0.012(1)
O (7)	24f	0.8955(4)	0.1789(4)	0.9992(19)	1	0.032(2)
La _{0.9} Ba _{0.1} Mn _{0.96} O _{2.41} - Space Group: <i>I23</i> (#197) Formula weight = 230.05 g mol ⁻¹ $a = 15.9933(4)$ Å, volume = 4090.9(3) Å ³						
Radiation source: Neutron, $\lambda = 1.594$ Å X-ray, Cu K α_1 = 1.594 Temperature: Room temperature $\chi^2 = 1.936$; $wRp = 5.55$ %; $Rp = 5.16$ %.						

Table 2. Structural parameters from the refinement of La_{0.9}Ba_{0.1}Mn_{0.96}O_{2.41} simultaneously against X-ray and neutron powder diffraction data.

FIGURES

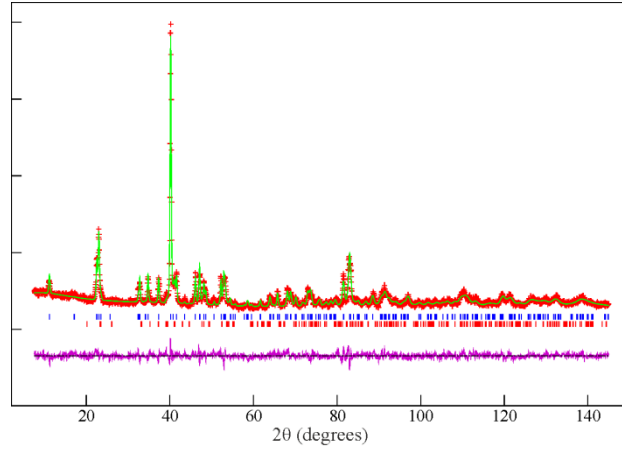


Figure 1. Observed, calculated and difference plots from the structural refinement of $\text{La}_{0.9}\text{Ba}_{0.1}\text{MnO}_{2.5}$ against neutron powder diffraction data collected at room temperature. Upper tick marks indicate peak positions for the majority phase, lower tick marks for the $\text{La}_{0.9}\text{Ba}_{0.1}\text{MnO}_3$ secondary phase.

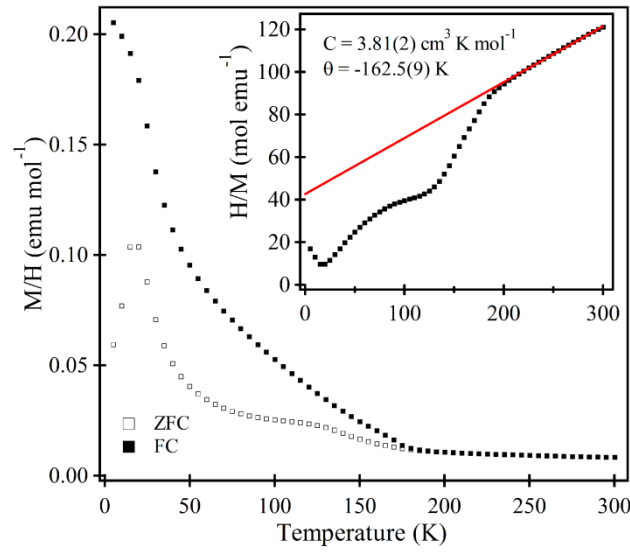


Figure 2. Magnetisation data collected from $\text{La}_{0.9}\text{Ba}_{0.1}\text{MnO}_{2.5}$ in an applied field of 100 Oe. In set shows the Curie-Weiss law fit to the ZFC data in the range $210 < T/\text{K} < 300$.

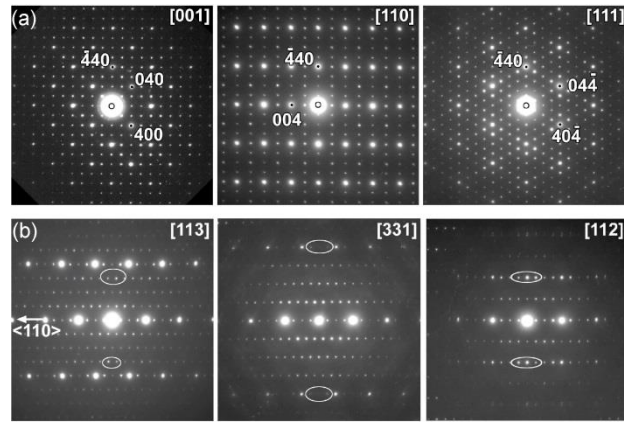


Figure 3. a) Electron diffraction patterns from the [001], [110] and [111] zone axes of ‘ $\text{La}_{0.9}\text{Ba}_{0.1}\text{MnO}_{2.41}$ ’ confirming the body-centred cubic unit cell. b) PED data collected from the [113], [331] and [112] zone axes of ‘ $\text{La}_{0.9}\text{Ba}_{0.1}\text{MnO}_{2.41}$ ’. Ovals highlight lack of mirror symmetry perpendicular to $\langle 110 \rangle$ which indicates the Laue class is $m\bar{3}$ not $m\bar{3}m$.

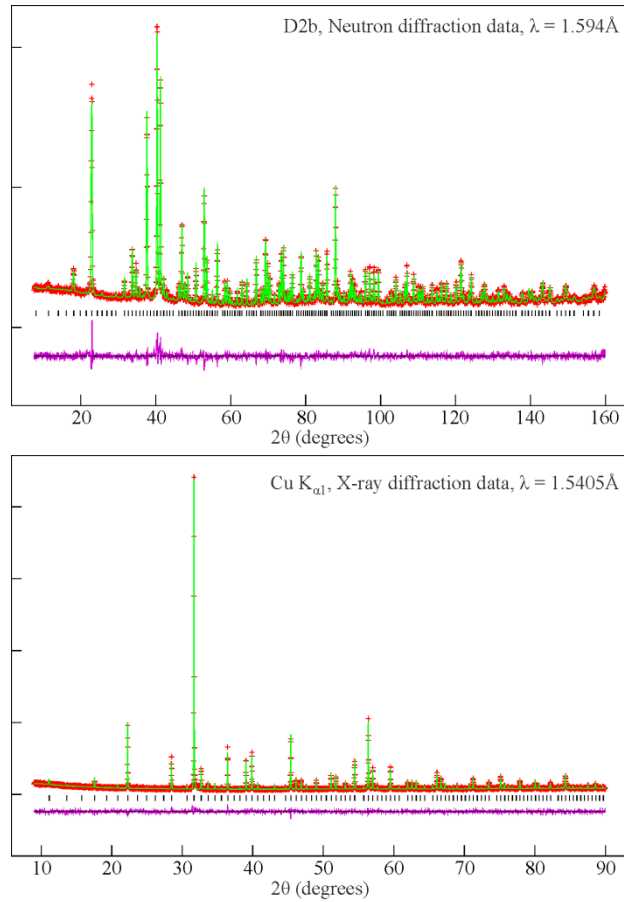


Figure 4. Observed, calculated, and difference plots from the simultaneous structural refinement of $\text{La}_{0.1}\text{Ba}_{0.9}\text{MnO}_{2.43}$ against neutron (top) and X-ray (bottom) powder diffraction data collected at room temperature.

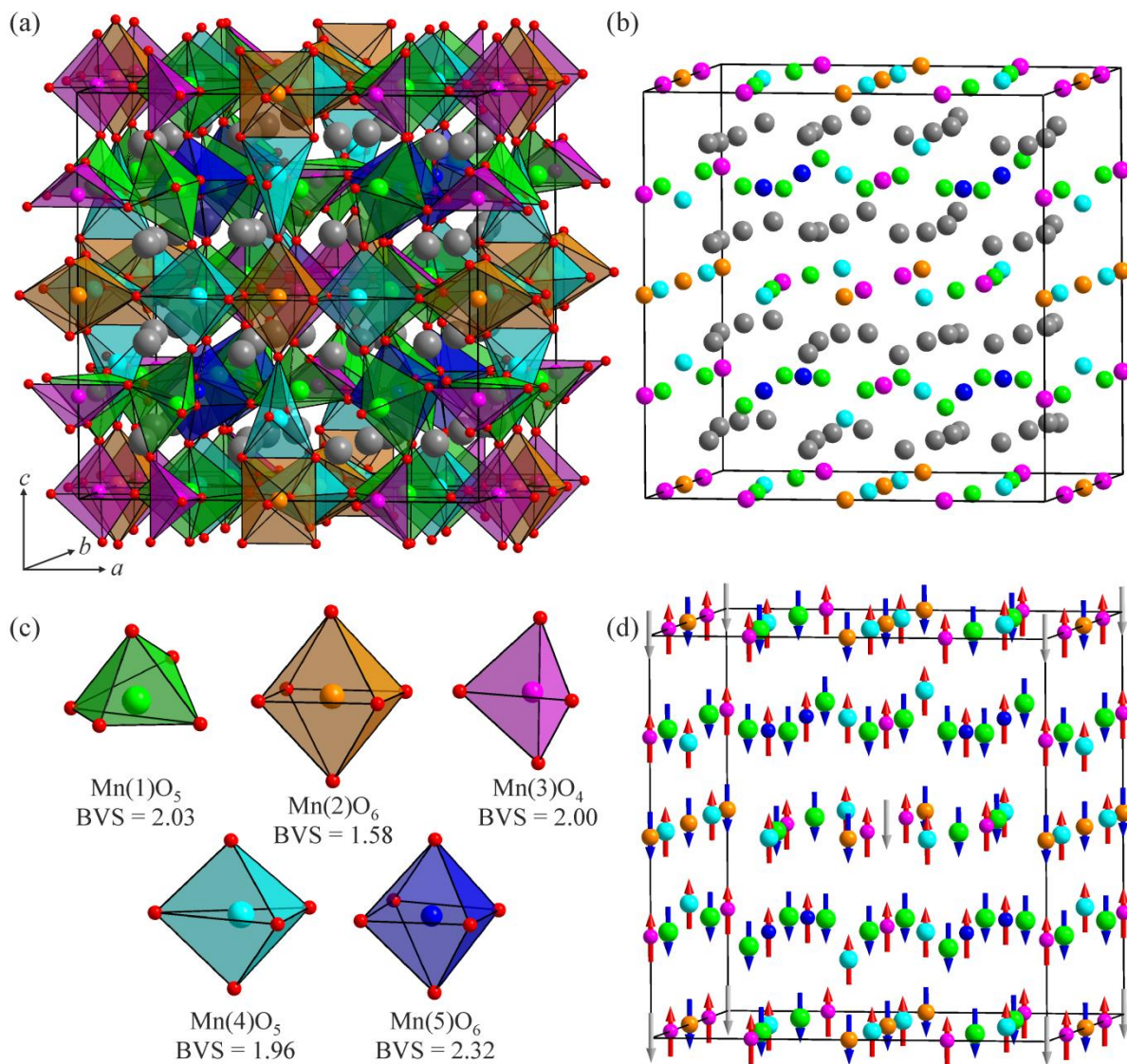


Figure 5 a) Complete crystal structure of $\text{La}_{0.9}\text{Ba}_{0.1}\text{Mn}_{0.96}\text{O}_{2.43}$, b) crystal structure of $\text{La}_{0.9}\text{Ba}_{0.1}\text{Mn}_{0.96}\text{O}_{2.43}$ without oxide ions, c) The local MnO_x coordination polyhedra present in $\text{La}_{0.9}\text{Ba}_{0.1}\text{Mn}_{0.96}\text{O}_{2.43}$. Grey and red spheres represent La/Ba and O respectively, with other colours representing Mn, as shown in (c). d) The magnetic structure of $\text{La}_{0.9}\text{Ba}_{0.1}\text{Mn}_{0.96}\text{O}_{2.43}$. Red and blue arrows indicate the orientation of the ordered moments of the manganese cations ($4.43(2) \mu\text{B}$). Grey arrows indicate the moments of the 'missing' manganese cations, if they adopted G-type antiferromagnetic order.

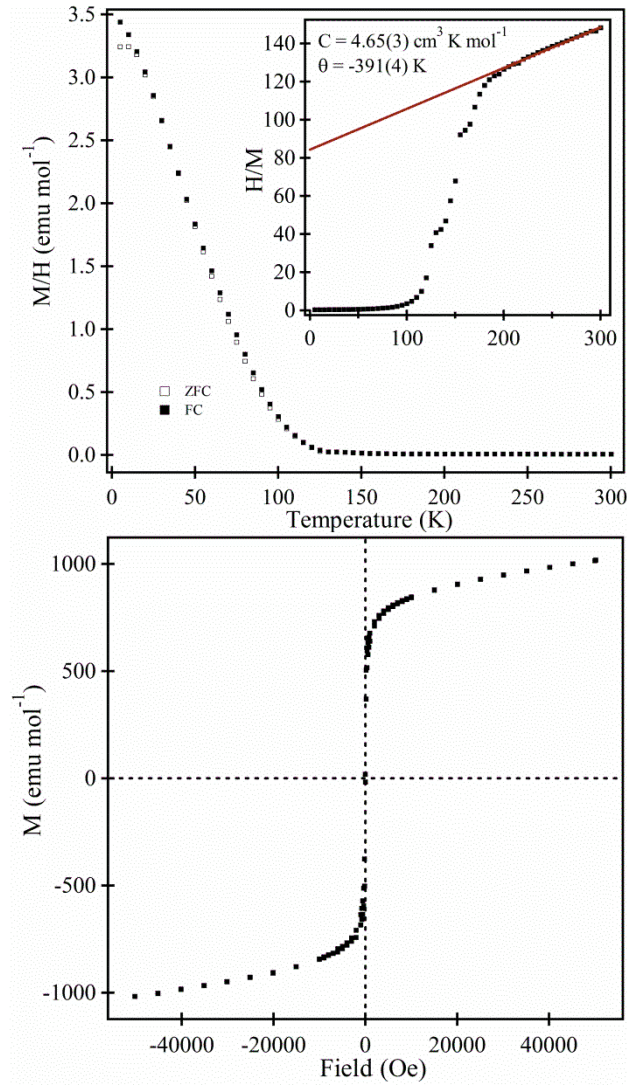


Figure 6. (top) Magnetisation data collected as a function of temperature from $\text{La}_{0.9}\text{Ba}_{0.1}\text{Mn}_{0.96}\text{O}_{2.43}$, inset shows fit to the Curie-Weiss law in the range $200 < T/\text{K} < 300$. (bottom) Magnetisation-field isotherm collected at 5 K after cooling in an applied field of 50000 Oe.

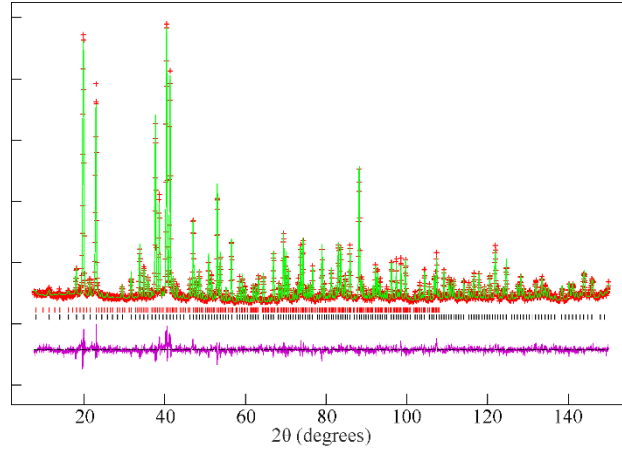


Figure 7. Observed, calculated, and difference plots from the structural and magnetic refinement of $\text{La}_{0.9}\text{Ba}_{0.1}\text{Mn}_{0.96}\text{O}_{2.43}$ against neutron powder diffraction data collected at 5 K. Lower tick marks indicate nuclear peak positions, upper tick marks magnetic peak positions.

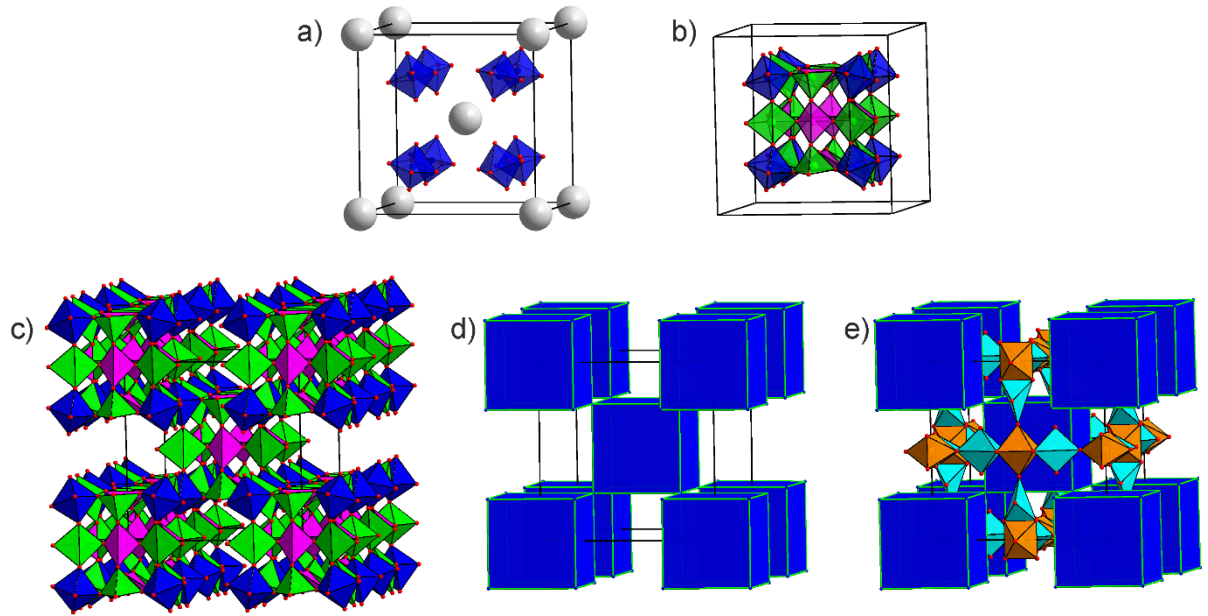


Figure 8. The structure of $\text{La}_{0.9}\text{Ba}_{0.1}\text{Mn}_{0.96}\text{O}_{2.43}$. a) a cube of $\text{Mn}(5)\text{O}_6$ octahedra surround each Mn-cation vacancy site b) $\text{Mn}(5)\text{O}_6$ units link with $\text{Mn}(1)\text{O}_5$ and $\text{Mn}(3)\text{O}_4$ units to form cubes, which link corners to form a network as shown in c) and schematically in d). e) Bands of edge and corner shared $\text{Mn}(2)\text{O}_6$ and $\text{Mn}(4)\text{O}_5$ units run between the cubes. Color scheme shown in Figure 5.